Performance Evaluation of PI and Sliding Mode Control for PMSM in Applications for Electric Vehicles

Kamel Cherif
Automatic Research Laboratory (LARA), National Engineering School of Tunis, University of Tunis El Manar, BP37, 1002 Tunis, Tunisia
kam.cherif@yahoo.fr (corresponding author)

Abdelaziz Sahbani
Automatic Research Laboratory (LARA), National Engineering School of Tunis, University of Tunis El Manar, BP37, 1002 Tunis, Tunisia
abdellazizsahbani@yahoo.fr

Kamel Ben Saad
Automatic Research Laboratory (LARA), National Engineering School of Tunis, University of Tunis El Manar, BP37, 1002 Tunis, Tunisia
kamel.bensaad@enit.utm.tn

Received: 29 February 2024 | Revised: 1 April 2024 | Accepted: 16 April 2024

Licensed under a CC-BY 4.0 license | Copyright (c) by the authors | *DOI: https://doi.org/10.48084/etasr.7172*

ABSTRACT

Electrical and mechanical subsystems are the main parts of the powertrain of an Electric Vehicle (EV). These parts include principally electric motors, inverters, batteries, wheels, axles, differentials, and transmissions. Permanent Magnet Synchronous Motor (PMSM) is one of the most popular used motors in the electric powertrain due to its several benefits over other AC motors, such as its small size, low weight, wide range of speed, elevated overload capacity, elevated power factor, and elevated efficiency. This paper compares the performance of PI and sliding-mode controllers for PMSM employed in electric vehicle applications with single-motor drive configurations. Dynamic performance and robustness are the main topics of the comparative analysis. The robustness of the drive train with sliding-mode controller is proven by simulation results.

Keywords-electric vehicle; powertrain; PMSM; sliding mode control; robustness

I. INTRODUCTION

Electric Vehicles (EVs) can be driven by one or more electric motors. Due to the differences of electric drive systems, such as the use of one electric motor or dual motor architecture, there are various EV architectures [1-3]. One motor-based powertrains are mostly preferred due to their ability to optimize the utilization of current mechanical systems in traditional automobiles. Thus, this one-motor architecture is the most commercialized for EVs [4]. In this paper, the focus is placed on the analysis and the modeling of an EV system that utilizes a single motor. Permanent Magnet Synchronous Motor (PMSM) is a common type of electrical motor implemented in EVs. It is a beneficial solution for powertrains as it has high overload capacity and high torque mass compared to the conventional asynchronous and synchronous motors [5].

Many articles in the literature have studied and tested the control of PMSM motors. Nevertheless, only few of them concentrate on applications on EVs. Authors in [6] demonstrate that the PI controller achieves a more robust tracking response of the command speed with a less steady-state error than the PID controller does. Authors in [7] suggest combining Sliding Mode Control (SMC) and fuzzy PI control in a system. Authors in [8] compare SMC and PI control for applications in lightweight EVs. The simulation results reveal the performances of the drive train of EV using SMC in terms of robustness and speed response. Authors in [9] propose a combination of Look-up table-based Field Oriented Control (FOC) with SMC for EV applications. The results confirm that the SMC scheme is more robust than that of the PI controller. Authors in [10] propose a sliding mode torque controller that can decouple q-axis and d-axis currents to rapidly track the reference torque. The suggested method guarantees a robust

control of PMSMs under model parameters and load torque variations.

Most studies on the topic are applied in lightweight EVs. That is why, in this paper, focus is given on a real EV. PI and SMC strategies are applied to an EV powertrain based on PMSM. Its robustness is tested against some disturbances such as parametric variation by changing the value of the acting forces on the EV body.

II. DESCRIPTION AND MODELING OF THE STUDIED SYSTEM

A. Forces Applied to a Moving Vehicle

The configuration of the studied EV, represented in Figure 1, contains a battery unit, an inverter, a PMSM with its mechanical parts (gearbox, axle, wheels, etc.), and a control unit [11].

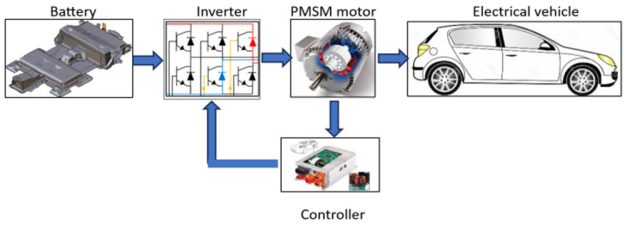

Fig. 1. The examined EV powertrain.

When an electric vehicle is moving on a slope road, it will be subjected to multiple forces, such as aerodynamic drag force, rolling resistance force, acceleration force and a gradient force as observed in Figure 2.

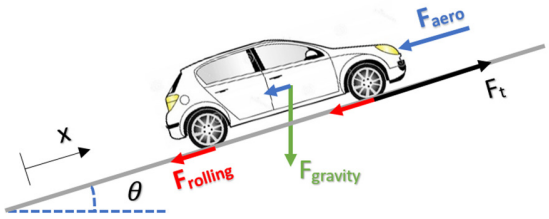

Fig. 2. Forces acting on the vehicle.

The dynamic equation of a vehicle motion along its longitudinal direction can be expressed as [11, 12]:

$$\sum F = m\ddot{x} = F_{\mathrm{t}} - F_{\mathrm{aero}} - F_{\mathrm{rolling}} - F_{\mathrm{gradient}} \quad (1)$$

where m is the total mass of the vehicle, $\ddot{x}$ is the acceleration, and F_{t} is the total traction force needed to drive the vehicle.

1) Rolling Resistance Force

The force required to overcome the rolling resistance can be calculated by :

$$F_{rolling} = C_{rr}.m.g \quad (2)$$

where g is the gravity acceleration, and C_{rr} is the coefficient of rolling resistance.

2) Aerodynamic Drag Force

$$F_{Aerodynamic\_Drag} = \frac{1}{2}.\rho.(V + Vw)^2.C_d.A_f \quad (3)$$

where A_f, ρ, and C_d are the vehicle frontal surface, the air density, and the air resistant coefficient, respectively. V and Vw stand for the vehicle velocity and wind velocity, accordingly.

3) Gradient Resistance Force

The gradient resistance force is expressed by:

$$F_{gradient} = m.g.\sin\theta \quad (4)$$

where θ is the inclination angle of the road.

B. Electric Traction Model

The electrical equations of a PMSM in dq-axis can be expressed as:

$$V_d = R_s I_d + L_d \frac{dI_d}{dt} - \omega L_q I_q \quad (5)$$

$$V_q = R_s I_q + L_q \frac{dI_q}{dt} + \omega(L_d I_d + \varphi_f) \quad (6)$$

where R_s *is* the phase resistance, L_q is the direct quadrature inductance, and φ_f is the flux linkage. The fluxes equations are expressed as:

$$\varphi_d = L_d I_d + \varphi_f \quad (7)$$

$$\varphi_q = L_q I_q \quad (8)$$

The electromagnetic torque is defined by :

$$C_{em} = \frac{3}{2}p(\varphi_d I_q - \varphi_q I_d) \quad (9)$$

The PMSM simplified electrical model can be represented as:

$$[V] = [R][I] + [L]\frac{d}{dt}[I] + \omega([A][I] + [\varphi]) \quad (10)$$

where:

$$[V] = \begin{bmatrix} V_d \\ V_q \end{bmatrix} : [R] = \begin{bmatrix} R_s & 0 \\ 0 & R_s \end{bmatrix} : [I] = \begin{bmatrix} I_d \\ I_q \end{bmatrix}$$

$$[L] = \begin{bmatrix} L_d & 0 \\ 0 & L_q \end{bmatrix} ; [A] = \begin{bmatrix} 0 & L_q \\ L_d & 0 \end{bmatrix} : [\varphi] = \begin{bmatrix} 0 \\ \varphi_f \end{bmatrix}$$

C. Coupling of Electrical and Mechanical Models

The actuator power is connected to the vehicle dynamic component via a gearbox. It has to be adjusted in a way that ensures that the machine's electrical shaft and wheels rotate at a a suitable speed and that the transmittable torque is always higher than the torque applied to the load. The following two equations result from a decrease in speed:

$$C_{em} = \frac{C_{em\ (wheel)}}{\eta_{red}.n} \quad (11)$$

$$\Omega_m = \Omega_{(wheel)}.n \quad (12)$$

The mechanical transmission equation may be written as:

$$J\frac{d\Omega_m}{dt} + f\Omega_m = C_{em} - C_r \quad (13)$$

where ω_m is the rotor mechanical speed, C_r is the external load torque, J is the moment of inerta, and f is the friction constant.

The machine load torque is defined by:

$$Cr = \frac{C_{r\ (wheel)}}{\dot{\eta}_{red}.n} \quad (14)$$

III. CONTROL OF THE STUDIED SYSTEM

Figure 3 illustrates the control techniques applied to a PMSM of the studied electric vehicle. The schematic diagram outlines the two speed control strategies, PI control and SMC.

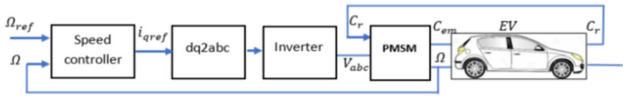

Fig. 3. Block diagram of the speed control strategies.

A. PI Control

The objective of this controller is to swiftly modify the active power in response to changes in the reference speed or the load torque, which in turn modifies the motor speed. The controller must simultaneously lower the variation in the active power value in a steady state while minimizing the variations in the stator current and electromagnetic torque. When a controller with constant control parameters is utilised, the two needs frequently collide. Under different kinds of speed oversight, a controller needs to be able to adjust the controller parameter values [6].

B. First Order Sliding Mode Control

The SMC method is acknowledged as an effective technique for crafting robust controllers suited for intricate, high-order nonlinear dynamic systems that operate amidst conditions of uncertainty [13, 14].

1) Controller Design

There are two parts to the SMC arrangement: one for perfect linearization (u_q) and one for stability (u_n). Control over the sliding mode is given by:

$$u = u_q + u_n \quad (15)$$

Its purpose is to store the control variable for the sliding surfaces $S(x)$. The corresponding control is obtained by assuming that the derivation of the surface is null: $\dot{S}(x) = 0$. u_n is the discrete control that assures convergence in the sense that:

$$S(x).\dot{S}(x) < 0 \quad (16)$$

So:

$$u_n = k.\text{sign}(S) \quad (17)$$

The gain function denoted by sign (S) is defined by :

$$\text{sign}(S) = \begin{cases} -1 \text{ if } S < 0 \\ 1 \text{ if } S > 0 \end{cases}$$

The commutations of the discrete control may cause chattering at high frequencies. This problem leads to a decrease in the performance of the first order sliding mode controller. The vector control approach is adopted to produce maximum electromagnetic torque output, specifically, $i_{dref} = 0$. Three control loops are provided: two current control loops, i_q and i_d, and a speed control loop [15-17].

2) The Speed ControlLloop

The control loop demands the employment of a speed reference Ω_{ref} and develops a current control i_q.

$$S(\Omega) = \Omega_{ref} - \Omega \quad (18)$$

$$\dot{S}(\Omega) = \dot{\Omega}_{ref} - \dot{\Omega} \quad (19)$$

The mechanical equation yields:

$$\dot{\Omega} = \frac{1}{J}(C_{em} - C_r) - \frac{f}{J}\Omega \quad (20)$$

Substituting (18) and (19) into (20), gives:

$$\dot{S}(\Omega) = \dot{\Omega}_{ref} - \frac{1}{J}\left[P\varphi_f i_q + P(L_d - L_q) i_d i_q\right] + \frac{C_r}{J} + \frac{f}{J}\Omega \quad (21)$$

with:

$$i_q = i_{q(eq)} + i_{q(n)}$$

While in sliding mode:

$$\dot{S}(\Omega) = 0 \; et \; i_{q(n)} = 0$$

Therefore:

$$i_{q(eq)} = \frac{J}{P\varphi_f + P(L_d - L_q) i_d}.\dot{\Omega}_{ref} + \frac{f}{P\varphi_f + P(L_d - L_q) i_d}.\Omega + \frac{1}{P\varphi_f + P(L_d - L_q) i_d}.C_r \quad (22)$$

In both the steady state and the convergence mode:

$$i_{q(n)} = k_1.\text{sign}(S(\Omega)) \quad (23)$$

where k_1 is a positive constant.

The purpose speed controller for the current study can be constructed as:

$$i_{q(n)} = -k_{p1}.|S(\Omega)|^{\frac{1}{2}}\text{sign}(S(\Omega)) + i_{q(n1)} \quad (24)$$

$$\frac{di_{q(n1)}}{dt} = -k_{i1}.\text{sign}(S(\Omega)) \quad (25)$$

where k_{p1} and k_{i1} are positive constants.

3) A Current i_q Control Loop

This control loop necessitates the use of a reference current i_{qref} and provides a control voltage V_q.

$$S(i_q) = i_{qref} - i_q \quad (26)$$

$$\dot{S}(i_q) = \dot{i}_{qref} - \dot{i}_q \quad (27)$$

$$\dot{i}_q = \frac{V_q - P\Omega L_d i_d - P\Omega\varphi_f - R_s i_q}{L_d} \quad (28)$$

During the sliding mode: $\dot{S}(i_q) = 0$

Therefore:

$$V_{q(eq)} = R_s i_q + P\Omega L_d i_d + L_q i_{qref} + P\Omega\varphi_f \quad (29)$$

During the convergence mode :

$$V_{q(eq)} = k_2.\text{sign}(S(i_q)) \quad (30)$$

where k_2 is a positive constant.

The current regulator is written as:

$$V_{q(n)} = -k_{p2}.|S(i_q)|^{\frac{1}{2}}\text{sign}\left(S(i_q)\right) + V_{q(n1)} \quad (31)$$

$$\frac{dV_{q(n1)}}{dt} = -k_{i2}.\text{sign}\left(S(i_q)\right) \quad (32)$$

where k_{p2} and k_{i2} are positive constants.

4) Current i_d Control Loop

This control loop involves the use of a reference current i_{dref} and delivers a control voltage V_d.

$$S(i_d) = i_{dref} - i_d \quad (33)$$

$$\dot{S}(i_d) = \dot{i}_{dref} - \dot{i}_d \quad (34)$$

Again:

$$\dot{i}_d = \frac{V_d + P\Omega L_q i_q - R_s i_d}{L_d} \quad So \quad (35)$$

$$V_{d(eq)} = R_s i_d - P\Omega L_q i_q + L_d \dot{i}_{dref} \quad (36)$$

$$V_{d(n)} = k_3.\text{sign}(S(i_d)) \quad (37)$$

where k_3 is a positive constant.

The direct current controller of the STSM can be represented as:

$$V_{d(n)} = -k_{p3}.|S(i_d)|^{\frac{1}{2}}\text{sign}\left(S(i_d)\right) + V_{d(n1)} \quad (38)$$

$$\frac{dV_{d(n1)}}{dt} = -k_{i3}.\text{sign}\left(S(i_d)\right) \quad (39)$$

where k_{p3} and k_{i3} are positive constants.

IV. APPLICATION TO EV AND SIMULATION RESULTS

In the vehicle system model, constant torque is applied as an input to get the speed of the vehicle. The vehicle dynamical system was simulated with the characteristics listed in Table I.

TABLE I. PEUGEOT 208 ELECTRIC PARAMETERS

Parametes	Value
Vehicle mass (m)	1455 kg
Weel radius (r)	0.279 m
Front Axle (df)	1 m
Rear Axle (dr)	1.346 m
Rolling Resistance (crr)	0.013
Drag Coefficient Cd	0.3
Air Density (ρ)	1.225 kg/m^3
Air resistance coefficient (C_A)	0.82
Vehicle frontal area (A_f)	1.2 m^2
Gravity (g)	9.81 m/s^2

A. Simulation Results

The reference speed chosen for all simulations is 100 rad/s, given that the PMSM motor starts unloaded. At t = 0.6 s a load of 11.56 N.m is applied.

1) Speed Responses

Figures 4 and 5 disclose the response of the PMSM motor driving an EV whose speed is controlled by the PI controller and the SMC controller, respectively. In the case of the PI controller, the speed response exhibits an oscillation until the speed settles at 0.3 s. There is also an overshoot, and after 0.3 s, the system settles at the reference speed. The vector control unit, which produces switching pulses for the PWM inverter powering the PMSM drive, receives input from the SMC, which also serves as a speed regulator. The SMC PMSM's speed response is noticed in Figure 5 in which the stabilization time is much shorter than that of the PI controller, and with no overshoot. It is therefore better than the PI controller for speed control. The SMC acts as an excellent speed controller.

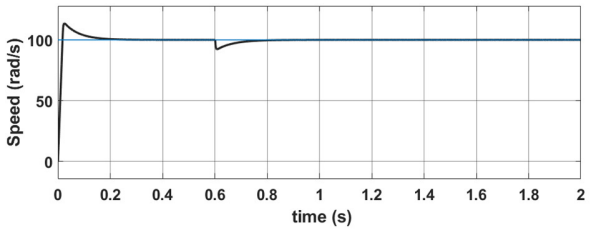

Fig. 4. Speed response of the PI controller.

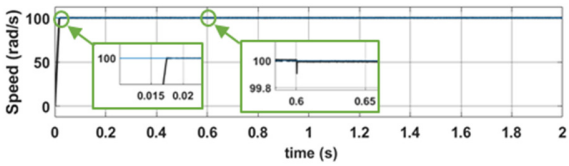

Fig. 5. Speed response of SMC.

2) Electromagnetic Torque

The torque developed by the PMSM motor (Te) is spotted in Figures 6 and 7. When the selected controller takes some time to settle at the reference speed, the initial torque is fairly powerful, and the created torque decreases after the fixed speed is attained. Initially, the motor is unloaded. At 0.6 s, a load torque of 11.56 N.m is applied.

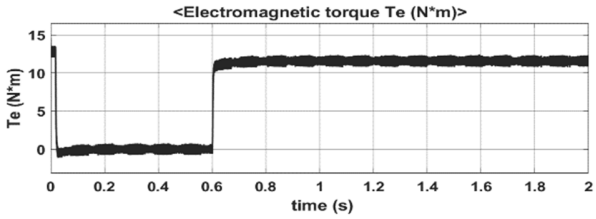

Fig. 6. Electromagnetic torque with PI control.

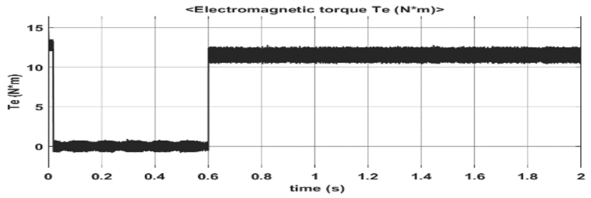

Fig. 7. Electromagnetic torque with SMC.

3) Three-phase Current responses

Figures 8 and 9 portray the three-phase stator current. The PMSM motor consumes a high current at start-up when the selected controller takes some time to settle at the reference speed, and the current drops to zero (the motor starts without load) once the set speed is obtained. When a load of 11.56 N·m is applied at 0.6 s, the current assumes the nominal value. Figures 10 and 11 depict the stator current.

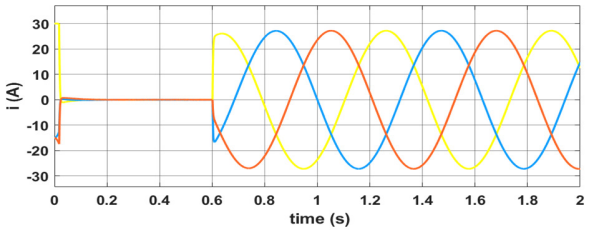

Fig. 8. Three-phase current response with PI controller.

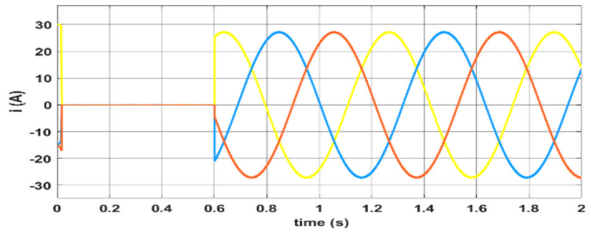

Fig. 9. Three-phase currents response with SMC.

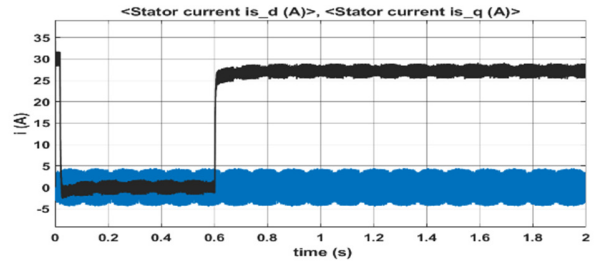

Fig. 10. Stator currents with PI controller.

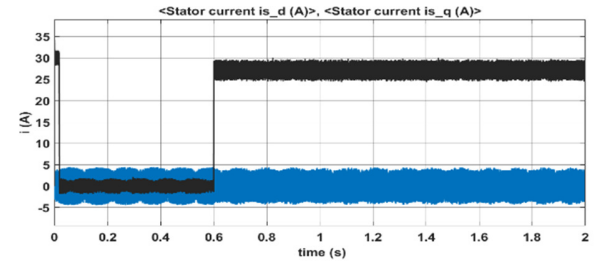

Fig. 11. Stator currents with SMC.

It should be noted that the obtained SMC three-phase current response is better than the one acquired by the PI control. Compared to the PI control, the SMC three-phase current response is smoother.

V. ROBUSTNESS TEST

The PMSM motor starts without load. At $t = 0.6$ s a load is applied (6). To test the robustness of the chosen controller, this research will act on F_{aero} or $F_{rolling}$ in (7).

A. $F_{rolling}$ Decreases by 45 N at t = 1 s

Figures 12 and 14 manifest the response of the PMSM motor driving an EV whose speed is controlled by the PI controller and the SMC, respectively. The corrsponding electromagnetic torque is illustrated by the characteristics in Figures 13 and 15. In the case of the PI controller, the speed response (Figure 12) indicates that after this disturbance, it takes 190 ms for the system to return to the reference speed. For the SMC, on the other hand, the speed response (Figure 14) takes no further than 90 ms to return to the reference speed after the same disturbance.

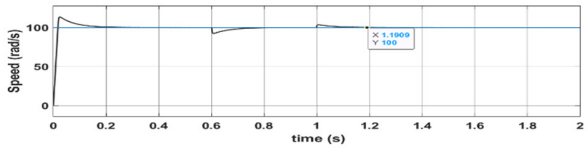

Fig. 12. Speed response curve of PI controller.

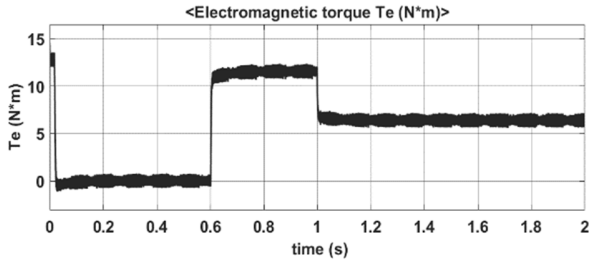

Fig. 13. Electromagnetic torque with the PI controller.

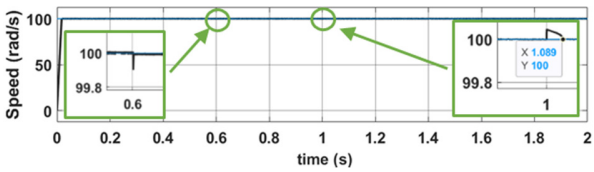

Fig. 14. Speed response with SMC.

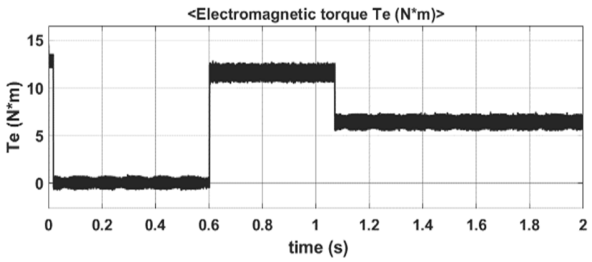

Fig. 15. Electromagnetic torque with SMC.

B. F_{aero} Decreases by 45 N at t=1 s

When the PI controller is applied, the speed response (Figure16) shows that after this disturbance, it takes 203 ms for the system to return to the reference speed. With SMC (Figure 18), the time taken to return to reference speed after the same disturbance is almost half of that of the PI controller.

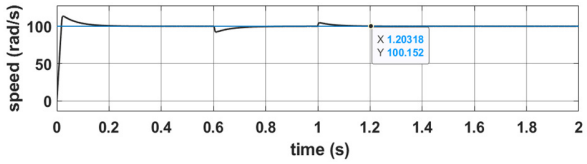

Fig. 16. Speed response curve of the PI controller.

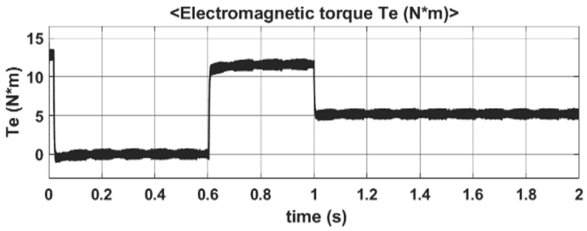

Fig. 17. Electromagnetic torque with PI the controller.

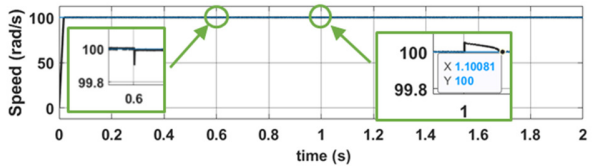

Fig. 18. Speed response curve of the SMC.

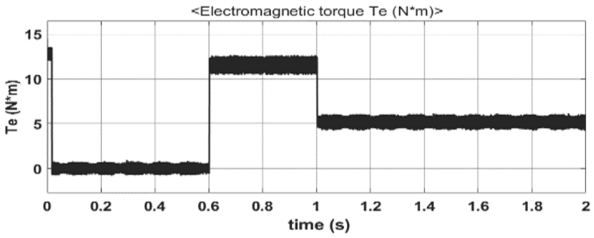

Fig. 19. Electromagnetic torque with the SMC.

C. ANOVA Test

In Figures 16-18, the disturbance is applied only at t = 1 s, and the time (Δt) taken to return to the reference speed is about 203 ms for PI controller and only 100 ms for SMC controller. For more robustness tests, with each considered controller, this study either increases or decreases the F_{aero} or F_{rolling} values by 45 N and notes the time (Δt) taken for the system to reach the reference. The results are provided in Table II. The present study has also performed one-way analysis of variance (ANOVA test) on response times between PI and SMC controllers.

The results drawn are statistically evaluated using ANOVA in order to assess their reliability. After the disturbances for each controller (PI and SMC), mean time and p-value (statistical concept in hypothesis testing) are calculated. The p-value obtained from the test is less than the significance level (α) of 0.05. It is concluded that there is a substantial difference in response times between PI and SMC controllers. The results reveal that the SMC is more robust than the PI controller.

VI. CONCLUSION

This research work presents a mathematic model of EV propulsed by PMSM. A comparative study of two control methods applied to an EV powertrain based on PMSM, was conducted. The proposed control strategies are PI control and SMC. The simulation results suggest that SMC outperformed the PI control. It gave better results with no overtaking and reached the reference speed in less time. To validate the derived results, the ANOVA test was performed on response times between PI and SMC. It is concluded that the results confirmed the robustness of the SMC.

REFERENCES

[1] H. Vidhya and S. Allirani, "A Literature Review on Electric Vehicles: Architecture, Electrical Machines for Power Train, Converter Topologies and Control Techniques," in *2021 International Conference on Computational Performance Evaluation (ComPE)*, Shillong, India, Sep. 2021, pp. 565–575, https://doi.org/10.1109/ComPE53109.2021.9751896.

[2] M. Hussain, A. Ulasyar, H. S. Zad, A. Khattak, S. Nisar, and K. Imran, "Design and Analysis of a Dual Rotor Multiphase Brushless DC Motor for its Application in Electric Vehicles," *Engineering, Technology & Applied Science Research*, vol. 11, no. 6, pp. 7846–7852, Dec. 2021, https://doi.org/10.48084/etasr.4345.

[3] B. Krüger, G. Keinprecht, G. Filomeno, D. Dennin, and P. Tenberge, "Design and optimisation of single motor electric powertrains considering different transmission topologies," *Mechanism and Machine Theory*, vol. 168, Feb. 2022, Art. no. 104578, https://doi.org/10.1016/j.mechmachtheory.2021.104578.

[4] W. Cai, X. Wu, M. Zhou, Y. Liang, and Y. Wang, "Review and Development of Electric Motor Systems and Electric Powertrains for New Energy Vehicles," *Automotive Innovation*, vol. 4, no. 1, pp. 3–22, Feb. 2021, https://doi.org/10.1007/s42154-021-00139-z.

[5] K. Kakouche, A. Oubelaid, S. Mezani, D. Rekioua, and T. Rekioua, "Different Control Techniques of Permanent Magnet Synchronous Motor with Fuzzy Logic for Electric Vehicles: Analysis, Modelling, and Comparison," *Energies*, vol. 16, no. 7, Jan. 2023, Art. no. 3116, https://doi.org/10.3390/en16073116.

[6] M. Y. Veeresh, V. N. B. Reddy, and R. Kiranmayi, "Modeling and Analysis of Time Response Parameters of a PMSM-Based Electric Vehicle with PI and PID Controllers," *Engineering, Technology & Applied Science Research*, vol. 12, no. 6, pp. 9737–9741, Dec. 2022, https://doi.org/10.48084/etasr.5321.

[7] X. Liu, J. Zhao, S. Wang, and Q. Xiang, "Research on Sliding Mode Control and Fuzzy Control Strategies of Motor Drive System for New Energy Vehicles," in *2021 40th Chinese Control Conference (CCC)*, Shanghai, China, Jul. 2021, pp. 5971–5976, https://doi.org/10.23919/CCC52363.2021.9550587.

[8] B. Bendjedia, L. Baadj, and A. Ibrahimibrahimi, "Sliding Mode Control of PMSM Drive for Lightweight Electric Vehicles," in *2022 19th International Multi-Conference on Systems, Signals & Devices (SSD)*, Sétif, Algeria, Feb. 2022, pp. 2109–2114, https://doi.org/10.1109/SSD54932.2022.9955503.

[9] R. S. Akhil, V. P. Mini, N. Mayadevi, and R. Harikumar, "Modified Flux-Weakening Control for Electric Vehicle with PMSM Drive," *IFAC-PapersOnLine*, vol. 53, no. 1, pp. 325–331, Jan. 2020, https://doi.org/10.1016/j.ifacol.2020.06.055.

[10] S. Dandan, D. Yugang, and Z. Chengning, "Sliding Mode Controller for Permanent Magnetic Synchronous Motors," *Energy Procedia*, vol. 105,

pp. 2641–2646, May 2017, https://doi.org/10.1016/j.egypro.2017.03.765.

[11] K. Cherif, A. Sahbani, and K. B. Saad, "Control Approaches of Permanent Magnet Synchronous Motor Used for Electric Vehicle Power Train," in *2nd International Conference on Industry 4.0 and Artificial Intelligence (ICIAI 2021)*, Feb. 2022, pp. 83–87, https://doi.org/10.2991/aisr.k.220201.016.

[12] A. Mohan, S. Adwaith, A. Subair, A. Jose, and N. Joy, "Performance Analysis of a Complete EV Powertrain using a Controller and MATLAB Simulink," in *2022 IEEE International Power and Renewable Energy Conference (IPRECON)*, Kollam, India, Sep. 2022, pp. 1–8, https://doi.org/10.1109/IPRECON55716.2022.10059506.

[13] V. Utkin, A. Poznyak, Y. Orlov, and A. Polyakov, "Conventional and high order sliding mode control," *Journal of the Franklin Institute*, vol. 357, no. 15, pp. 10244–10261, Oct. 2020, https://doi.org/10.1016/j.jfranklin.2020.06.018.

[14] V. Utkin, J. Guldner, and J. Shi, *Sliding Mode Control in Electro-Mechanical Systems*, 2nd ed. Boca Raton, FL, USA: CRC Press, 2017.

[15] A. Pawar and S. V. Jadhav, "Sliding Mode Hybrid Control of PMSM for Electric Vehicle," in *Smart Sensors Measurement and Instrumentation*, 2023, pp. 165–181, https://doi.org/10.1007/978-981-19-6913-3_11.

[16] Q. Hou, S. Ding, and X. Yu, "Composite Super-Twisting Sliding Mode Control Design for PMSM Speed Regulation Problem Based on a Novel Disturbance Observer," *IEEE Transactions on Energy Conversion*, vol. 36, no. 4, pp. 2591–2599, Sep. 2021, https://doi.org/10.1109/TEC.2020.2985054.

[17] H. Alnami, C. Pang, and Q. Wang, "A Novel Sliding Mode Control Method of Interior-Mounted PMSM," in *2021 IEEE Texas Power and Energy Conference (TPEC)*, College Station, TX, USA, Oct. 2021, pp. 1–6, https://doi.org/10.1109/TPEC51183.2021.9384961.